Assembly mechanism of recombinant spider silk proteins

S. Rammensee*, U. Slotta[†‡], T. Scheibel[†‡§], and A. R. Bausch*[§]

*E27-Biophysics, Physics Department, James Franck Straße, and [†]Biotechnology, Chemistry Department, Lichtenbergstraße 4, Technische Universität München, 85747 Garching, Germany

Edited by David Baker, University of Washington, Seattle, WA, and approved March 13, 2008 (received for review October 5, 2007)

Spider silk threads are formed by the irreversible aggregation of silk proteins in a spinning duct with dimensions of only a few micrometers. Here, we present a microfluidic device in which engineered and recombinantly produced spider dragline silk proteins eADF3 (engineered *Araneus diadematus* fibroin) and eADF4 are assembled into fibers. Our approach allows the direct observation and identification of the essential parameters of dragline silk assembly. Changes in ionic conditions and pH result in aggregation of the two proteins. Assembly of eADF3 fibers was induced only in the presence of an elongational flow component. Strikingly, eADF4 formed fibers only in combination with eADF3. On the basis of these results, we propose a model for dragline silk aggregation and early steps of fiber assembly in the microscopic regime.

colloids | microfluidics | protein materials | rheology

Fibrous proteins are essential building blocks of life, providing scaffolds for cells, both intra- and extracellularly (1). Although most beneficial fibrous assemblies are formed reversibly, irreversible protein aggregation often leads to pathological conditions as found in a group of diseases, including Alzheimer's disease (AD), Parkinson's disease (PD), Huntington's disease (HD), and the transmissible spongiform encephalopathies (TSEs; prion diseases), all of which include extremely stable, highly ordered fibrils termed amyloids (2, 3). In these so-called conformational diseases, partial misfolding of the involved proteins results in uncontrolled aggregation. However, not every irreversible protein aggregation leads to disease. A wide range of biomaterials are based on extremely stable, extracellular protein fibrils without pathological characteristics. For controlled extracellular fiber formation in biomaterials such as silk, a tightly controlled aggregation and assembly process is mandatory. Upon production, the silk proteins are stored preliminarily under conditions preventing their aggregation in the spinning gland. To form stable self-assembled silk, aggregation of proteins is chemically and physically initiated in spinning ducts with dimensions of only a few micrometers (Fig. 1*a*). For silk spinning, two principally different models have been proposed previously. Whereas one model is based on the hypothetical presence of liquid crystalline flow properties of the spinning dope before fiber formation (2), the other model proposes intermediate colloidal assembly states as a prerequisite for fiber assembly (3). Unfortunately, the complexity of the *in vivo* process limits a detailed analysis of the assembly mechanism, and *in vitro* modeling has long been hampered because of the low amount of available highly purified spider silk proteins (4).

Producing engineered spider silk proteins recombinantly in bacteria provides, however, new possibilities for the investigation of spinning processes (5–7). In this work, we used eADF3 and eADF4, previously established engineered variants of the dragline silk fibroins ADF3 and ADF4 of the garden spider *Araneus diadematus* (8). One advantage of eADF3 and eADF4 is their easy accessibility at high purity [supporting information (SI) Fig. S1 and *Materials and Methods*]. Under distinct solvent conditions these engineered silk proteins controllably assemble into different morphologies, such as nanofibrils (6), hydrogels (7), films (9, 10), and microcapsules (11). Further, conditions for a liquid–liquid phase separation have been identified, leading to large colloidal assemblies that likely reflect a prerequisite for silk fiber formation (12).

Here, we focused on conditions for the controlled aggregation necessary for fiber formation in a laminar flow. In spiders, the spinning duct is a thin S-shaped channel of up to several centimeters in length (depending on spider species and body weight), surrounded by secretory cells that are involved in adjusting the ionic conditions and pH (13). Thus, flow conditions in spider glands can be technically best mimicked by microfluidic devices: laminar flow conditions enable precise control of ion concentrations and pH values along the channel, and elongational flow conditions can be easily adjusted. Different designs of microfluidic channels allow disentangling various effects, because the solvent conditions can be varied in respect to the various flow conditions and all processes can be observed optically in a time-resolved manner. Therefore, microfluidic devices enable examination of all parameters necessary for assembly of spider silk proteins.

The modular architecture of our microfluidic device (Fig. 1*b*) enables solvent adjustments similar to those found in nature by ion exchange and pH with different streams of liquids that are brought into contact. Further, an elongational flow component was applied by narrowing the channel width. Variation of the order of events in the microfluidic device allowed identifying the necessity of each individual contribution and the influence of the sequential order thereof.

Results and Discussion

Previously, it could be shown that eADF4 self-assembles into intracellular threads when produced in insect cells (14). Therefore, we first investigated the assembly of bacterially produced eADF4 in microfluidic channels. In these experiments, a stream of protein solution (10 mg/ml) was mixed with two streams of varying potassium phosphate concentrations and pH values. Surprisingly, no conditions were found for eADF4 to assemble into fibers: only spherical solid protein aggregates were formed under all conditions tested (15) (Fig. 2 *Left*).

Author contributions: T.S. and A.R.B. designed research; S.R. and U.S. performed research; U.S. contributed new reagents/analytic tools; S.R. analyzed data; and S.R., T.S., and A.R.B. wrote the paper.

The authors declare no conflict of interest.

This article is a PNAS Direct Submission.

[‡]Present address: Biomaterials, Fakultät für Angewandte Naturwissenschaften, Universitätsstraße 30, Universität Bayreuth, 95440 Bayreuth, Germany.

[§]To whom correspondence may be addressed. E-mail: abausch@ph.tum.de or thomas.scheibel@uni-bayreuth.de.

This article contains supporting information online at www.pnas.org/cgi/content/full/0709246105/DCSupplemental.

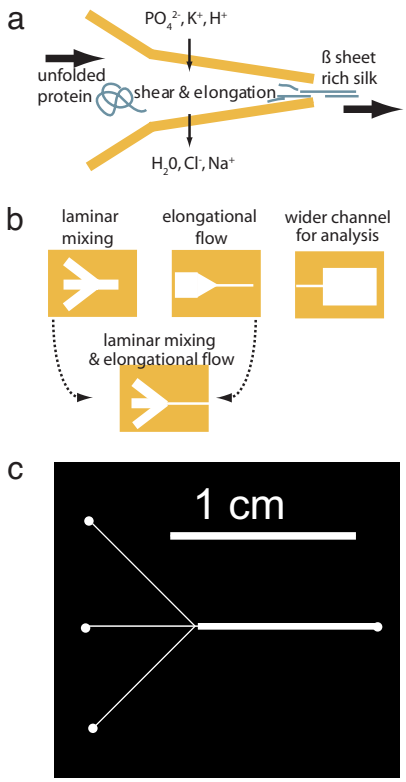

Fig. 1. Natural and artificial spinning ducts. (*a*) Schematics of the proposed natural spinning process of spider dragline silk. A highly concentrated protein solution is introduced and subjected to a hydrodynamic shear field. As the solution is pulled through the spinning duct, the pH is decreased (from slightly basic to slightly acidic pH). Further, phosphate and potassium ions (salting out) are added to the spinning dope. Simultaneously, water, sodium, and chloride (salting in) ions are extracted from the dope by the epithelium. The resulting silk fiber is rich in β-sheet secondary structure (29). (*b*) Components used in the microfluidic channels. (*Upper*) (*Left*) A laminar ''mixer'' module. Three streams of liquid are brought into contact. Mixing takes place only by diffusion. (*Center*) Elongational flow module. Narrowing the flow causes elongational flow components in the direction of the flow, resulting in the alignment of the molecules and fiber formation. (*Right*) Analysis module. A wider channel is placed at the end of the device to analyze the produced assemblies microscopically. (*Lower*) A setup that combines laminar mixing and elongational flow. It should be noted that the microfluidic devices presented here will not extract water, sodium, and chloride from the channel, but rely on diffusive mixing of the solutions. (*c*) Mask layout used for the formation of eADF3 fibers, combining the laminar flow mixing part and the elongational flow part (to scale). For fiber formation, the protein stream was introduced by the inlet in the middle left, and potassium phosphate solutions from the two outer inlets.

Because bacterially produced eADF3 has already been shown to form fibers *in vitro* (12), we next analyzed eADF3 in our microfluidic channels. It has been observed that eADF3 immediately forms spherical colloidal particles in 500 mM potassium phosphate. These particles typically have diameters of 1–5 μm (see Fig. 2 *Left*). In the microfluidic devices, we were additionally able to produce fibers. However, eADF3 fibers were found only when elongational flow (16), increase of phosphate concentration (to 500 mM), and pH drop to 6.0 were applied. eADF3 fiber formation started at a flow rate of 600 μl/h at a concentration of 20 mg/ml. Thus an elongational flow component $\dot{\varepsilon} = \partial v_x/\partial x$ of the order of 1,000 s^{-1} suffices to form eADF3 fibers at low protein concentrations.¶ At lower flow rates only spherical eADF3 colloidal aggregates have been observed, similar to aggregates in equivalent quiescent conditions (12). Under all other experimental conditions with lower phosphate concentrations, without elongational flow, or without pH drop, eADF3 assembled into spherical aggregates that slightly differed from those found for eADF4 (Fig. 2).

Analysis of the resulting eADF3 fibers revealed that they are highly flexible. eADF3 fibers could be stretched by increasing the flow in the direction of the fiber axis or collapsed by inverting the flow direction (Fig. 3). Analysis of the fibers in crossed-polarizers microscopy showed patches of structurally highly ordered molecules along the thread (Fig. 3). Their secondary structure content was observed by FTIR microscopy, which revealed that fibers produced in the microfluidic devices contain mainly β-sheets that are responsible for the ordered structural patches as seen in the crossed-polarizers spectroscopy (Table 1 and Fig. S2). Remarkably, eADF3 fibers were stable in Millipore water even in the absence of potassium phosphate or other ions. This is not the case for the spherical aggregates of eADF3, which disassembled upon replacement of the potassium phosphate buffer with distilled water.

As the described elongational flow is a necessary precondition for eADF3 fiber formation, the aberrant assembly behavior of eADF3 and eADF4 likely emerges from differences in their response to flow, that is, their rheological behavior. Therefore, we investigated the rheological properties of suspensions of spherical aggregates of eADF3 and eADF4 and determined their viscosity. Strikingly, drastic differences in the behavior of eADF3 and eADF4 were found: whereas suspensions of spherical aggregates of eADF4 flowed undisturbed under shear rates of 80–800 s^{-1}, suspensions of eADF3 spheres revealed the formation of higher-order aggregates under identical conditions, as indicated by the irreversible increase of the measured viscosity (Fig. 4). Further, aggregation of eADF3 was observed to occur faster with increasing shear rate (Fig. 4 *Left*). In the rheometer only shear flow is present. The flow in the microchannels, however, can be described as a shear flow at comparably low shear rates of 50 s^{-1}. Only in the bottlenecks is the superimposed elongational flow the dominating flow effect resulting in aggregation of eADF3.

In general, spherical colloidal assemblies are forced into contact when the respective streamlines of the solvent get closer than the diameter of the particles. Such behavior has been shown to be the dominant cause for aggregation for particles in the micrometer range (17) and to induce shear-activated irreversible aggregation (18). Once the colloidal silk spheres interact, the intrinsic characteristics of eADF3 and eADF4 contribute to a behavior that can be interpreted by a model originally developed for associative polymers in flow (19). Hydrophilic side chains presumably stick out of the spherical colloidal assemblies of eADF3 and form dangling ends that can interact with neighboring spherical colloidal assemblies (Fig. 5). If interactions are favored kinetically, shear thickening can be observed (19). Shear increases the collision rate of individual proteins or assemblies (20) by increasing the root-mean-square projection of the dangling end in the deformation direction. Such behavior was observed for eADF3 colloidal assemblies, which can interact during elongational flow upon increase of the hit rate of dangling ends (19). As a result viscosity increases over time, and a macroscopic clot of aggregated material forms (Fig. 4). Spherical colloidal assemblies of eADF3 revealed predominantly helical conformation, indicating that its conformational state is not that of the final fiber (21, 22) (Table 1). eADF3 aggregates can be resolved upon reducing the concentration of potassium phosphate (and its accompanying salting-out effect). Applied shear forces induce the irreversible aggregation of eADF3 into fibers with concomitant conformational change into β-sheet secondary

¶The elongational flow component is estimated from the averaged flow speed of v_x of 5 mm/s in the channels and of 160 mm/s in the narrow orifice. The distance between orifice and the onset of elongational flow is approximately 100 μm.

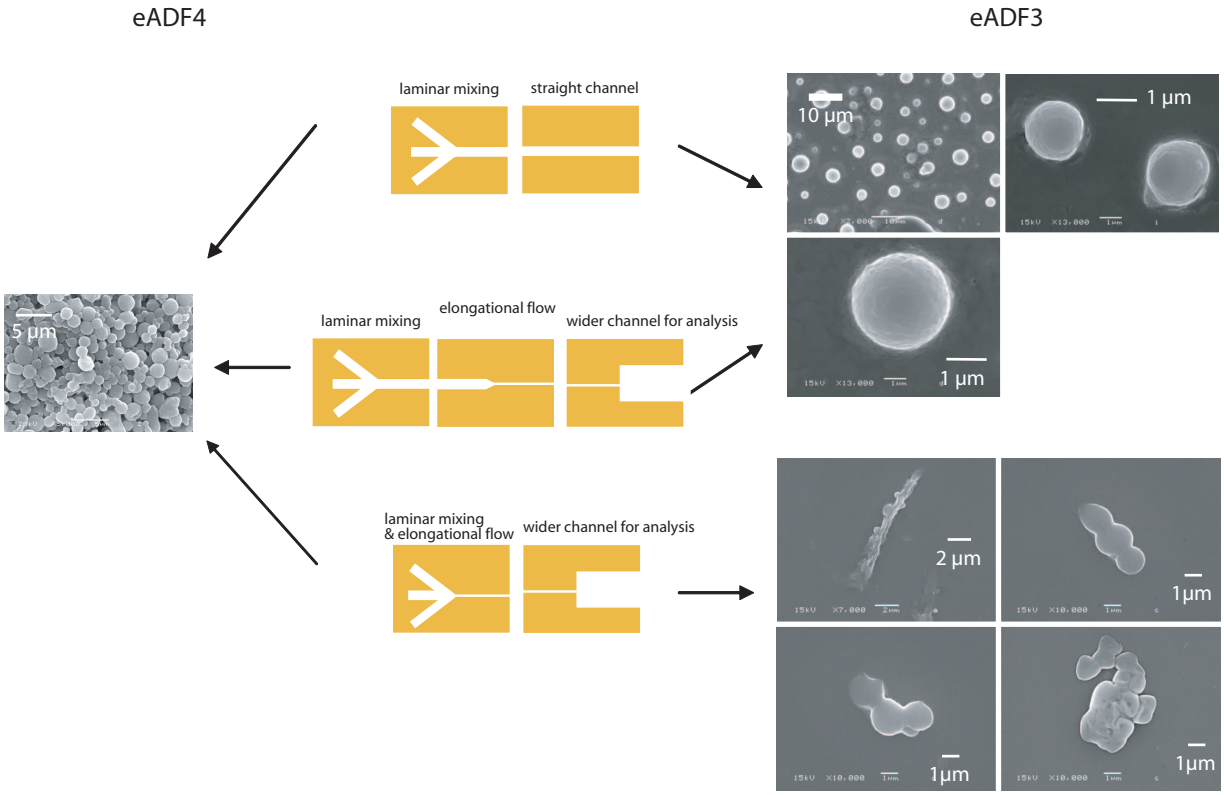

Fig. 2. Microfluidic setups used in this study and resulting eADF assemblies. (*Top*) A laminar flow mixing device. No elongational flow component is generated along the flow direction. (*Middle*) A laminar flow mixing device with a bottleneck 1,000 μm downstream of the laminar flow mixing region. A fluid element approaching from the left is subjected to an elongational flow just before the bottleneck. (*Bottom*) A laminar flow mixing device with a bottleneck at the point of mixing. An incoming flow element is subjected to elongational flow at the time of mixing with the fluids from the neighboring channels. Mixing always takes place by diffusion only. For eADF4, spherical colloidal assemblies are observed in all geometries. For eADF3, the third setup results in merged spherical assemblies and, depending on the flow rate, also in larger fibers, as shown in Fig. 3.

structure. Therefore, we assume that sphere formation is a prerequisite for fiber formation.

In contrast, for eADF4 addition of potassium phosphate (>300 mM) results in increased hydrophobic interactions accompanied by a dense packing of the proteins. Such tight packing leads to extremely smooth surfaces of the spherical colloidal assemblies. The high aggregation propensity of eADF4 results in the formation of chemically stable spheres in the presence of potassium phosphate (8), with a high content of β-sheet secondary structure (Table 1). The lack of dangling ends results in undisturbed flow of the eADF4 colloidal assemblies at the investigated shear rates and times (Fig. 4). Irreversible sphere formation of eADF4 occurs rapidly, and the accompanying conformational change of the protein is probably initiated in the center of the spheres (23). Thus, no further interaction between spherical colloidal eADF4 assemblies is possible, and no fiber assembly of eADF4 occurs (Figs. 2 and 5).

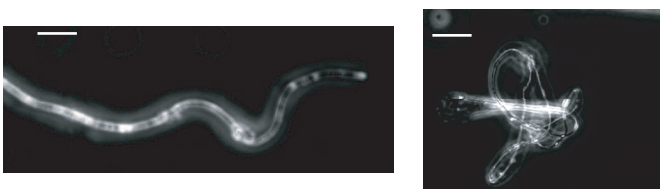

Fig. 3. Fibers of engineered spider silk proteins assembled in a microfluidic device: micrographs of fibrous eADF3 (in water). Dark and bright spots in crossed-polarizers microscopy reveal areas of higher and lower molecular orientation. By reversing the direction of flow in the microfluidic device, eADF3 fibers can be collapsed into small coils. Obtained fibers are quite flexible and able to bear large curvatures. (Scale bar: 10 μm.)

However, the presence of attractive interactions between eADF3 spheres alone is not sufficient for fiber formation. Fiber formation is observed only upon simultaneous decrease in pH from 8 to 6 and application of an elongational shear flow. When the solution of eADF3 was adjusted to pH 6 before initiating the elongational flow, no eADF3 fibers were formed (Fig. 6), and only spherical aggregates were observed. Because only the nonrepetitive carboxyl-terminal domain of eADF3 contains four amino acids with charged side chains, the necessity of pH change likely indicates the importance of the nonrepetitive domain for fiber assembly. Importantly, induction of colloidal assembly formation upon addition of potassium phosphate at pH 8 outside the microchannels did not affect fiber assembly: the preassembled microspheres converted into fibers when pH drop and elongational flow were applied simultaneously in the microfluidic device. Thus, the preformed spheres are forced together by elongational flow and the pH drop mediates irreversible structural conversion into β-sheet-rich fibers. These changes in secondary structure are similar to the assembly process of spider silk *in vivo* (21, 22, 24).

Because natural dragline silk consists of both eADF3 and eADF4, we finally investigated the impact of the second dragline silk protein (eADF4) on eADF3 fiber assembly. Therefore, we tested mixtures of the two proteins (eADF3:eADF4 weight ratios from 10:1 to 1:1) concerning its behavior in our microfluidic device. Strikingly, out of the mixture fibers assembled similar to those of eADF3 alone (Fig.

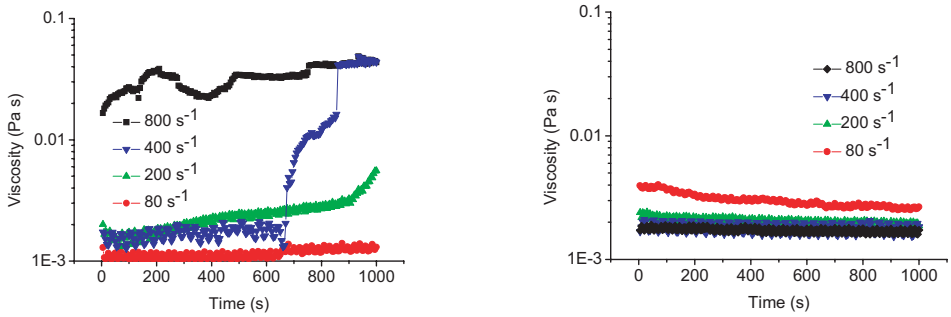

Fig. 4. Flow behavior of suspensions of eADF3 and eADF4 spherical aggregates. (*Left*) A suspension of eADF3 (10 mg/ml) preformed colloidal aggregates is subjected to various shear rates in a cone-and-plate rheometer. For low shear rates, no significant increase in the viscosity is recorded for up to 1,000 s. At high shear rates, an increase in the apparent viscosity indicates shear-induced aggregation of eADF3 solutions in the presence of 500 mM K_2HPO_4. The effect gets stronger with increasing shear rates. (*Right*) No effect of shearing is observed for eADF4 (10 mg/ml) in 500 mM K_2HPO_4.

7). To visualize the potential incorporation of eADF4, we partially labeled (10% wt/wt) eADF4 with the fluorescent dye FITC (9). Fluorescent micrographs revealed homogenously distributed eADF4 in the assembled fiber (Fig. 7).

It should be noted that the surface of the fibers obtained in the microfluidic channels contains grainy structures, in contrast to the very smooth surfaces of natural silk fibers. Presumably, the assembled structures represent early or intermediate stages of fiber formation, and likely also contain spherical aggregates formed during assembly. Also, it is important to keep in mind that the formation is taking place under water. Drying as found in the natural spinning process is not mimicked in this system and no postspinning drawing has been applied.

Conclusion

In summary, our results are in good agreement with the model of silk formation in insects proposed by Jin and Kaplan (3). We observe that colloidal aggregates are a prerequisite for fiber formation. The preaggregation leading to micrometer-size particles is necessary to allow shear-induced fiber assembly (17). Once the particles come into contact, their attractive interaction is highly important. Because the interaction between the eADF4 spherical aggregates is not sufficiently attractive, fiber formation of ADF4 does not occur.

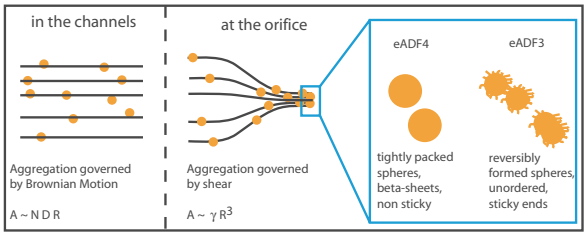

Fig. 5. Model for interaction of engineered spider silk proteins. Under moderate flow rates, Brownian motion dominates the aggregation of spherical protein colloidal assemblies. The aggregation rate *A* is proportional to the density of particles *N*, their radius *R*, and their diffusion constant *D*. In the proximity of the small orifice in the microfluidic device, particles traveling along the streamlines of the medium are forced into contact, drastically increasing the aggregation rate. Under these conditions, aggregation rate *A* is proportional to the shear γ and to the third power of the particles' radius *R* (17). eADF4 spherical colloidal assemblies are apparently ''smooth,'' no dangling ends stick out and contribute to sticking interactions with neighboring colloidal assemblies. In contrast, eADF3 spherical colloidal assemblies are supposed to have dangling ends, which can mediate interactions between neighboring aggregates (19, 20). Moreover, eADF3 spherical aggregates can be dissolved before aggregation into fibers. The rheological data presented in Fig. 4 support this model.

Importantly, only protein solutions of low or medium concentration have been used in this study, indicating that liquid crystalline behavior of the spinning dope is not a necessary prerequisite for fiber spinning under the conditions tested. However, high flow rates are necessary in our system to induce fiber assembly. In nature, extremely high protein concentrations and thus dramatically increased viscosities enable fiber formation at much lower elongational flow rates.

The presented approach combining modular microfluidic devices and protein engineering is a promising route to gain further insights into aggregation processes of silk and other proteins. For further analysis, the fibers produced with our method can be extracted from the microfluidic devices by flushing them out with water, enabling the more detailed investigation of structure–function relationships of the proteins. Such experiments could be performed with atomic force

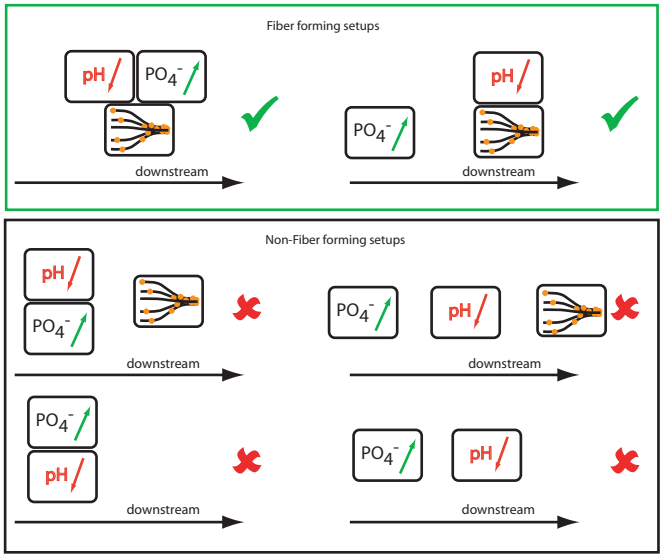

Fig. 6. Overview of the results on eADF3 assembly in microfluidic devices. (*Top*) Elongational flow, salting out, and pH changes are necessary for silk fiber formation. The induction of sphere formation by addition of phosphate occurs before the elongation flow. The pH drop, however, has to accompany elongational flow to induce the aggregation of the preformed spheres into fibers. Simultaneously with fiber formation, the secondary structure of the aggregates is changed to β-sheets. (*Middle*) If the pH is changed before elongational flow is applied, no fibers can assemble. The simultaneous pH drop and elongational flow is mandatory for fiber formation. (*Bottom*) If no elongational flow is applied, fibers do not form in any case. Elongational flows above 1,000 s^{-1} are necessary for fiber formation.

BIOPHYSICS

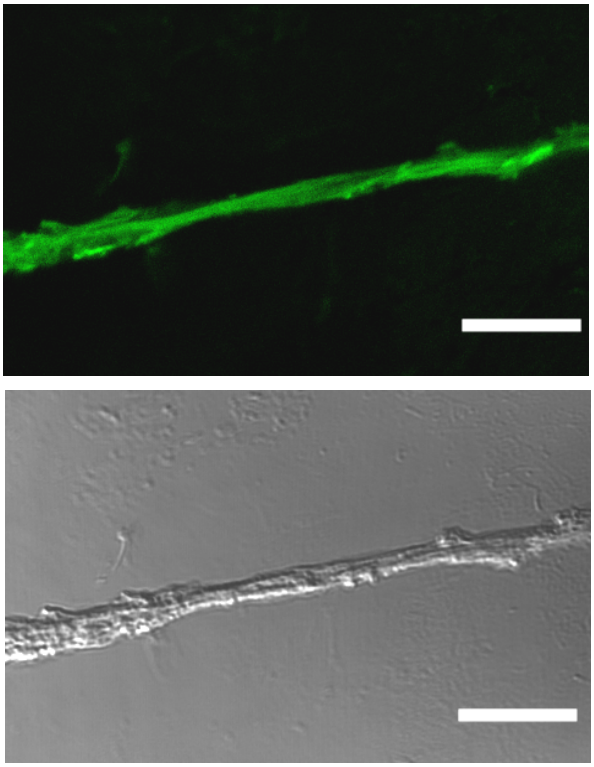

Fig. 7. eADF3/eADF4 mixed fibers. Micrographs show a dried fiber, consisting of both eADF3 and eADF4 (weight ratio 10:1). (*Upper*) Ten percent of the eADF4 protein was conjugated with the fluorescent dye FITC (equaling 1% of the total protein). Most FITC-labeled eADF4 has been homogenously integrated into the fiber, as seen by fluorescence microscopy. (*Lower*) Differential interference contrast micrograph of the same fiber. (Scale bar: 10 μm.)

microscopy or optical tweezers. An important issue for mechanical testing is fixing the short and thin fibers in a well defined way without destroying or altering their properties.

Materials and Methods

Proteins. Proteins were produced and purified as described previously (8) and lyophilized. Next, lyophilized proteins were dissolved in 6 M guanidinium thiocyanate and dialyzed into 10 mM tris(hydroxymethyl)aminomethane (Tris) buffer, titrated to pH 8 with HCl. Protein concentrations were measured by absorbance at 280 nm in an ND-1000 spectrophotometer (Nanodrop) using the calculated extinction coefficients of 73,950 $M^{-1}{\cdot}cm^{-1}$ for eADF3 and 46,400 $M^{-1}{\cdot}cm^{-1}$ for eADF4. Potassium phosphate buffers were prepared at 300 mM and 500 mM at pH 8 or 6.

Microfluidic Setup. Rapid prototyping of microfluidic devices cast of poly(dimethylsiloxane) (PDMS) was used (25). Briefly, the design of the device is printed in high resolution (3,000 dpi) on a transparency which is used as a mask to expose SU-8 50 positive photoresist (Microchem). After developing, the SU-8 structure serves as a master for the casting of PDMS, which is poured onto the master as a liquid. PDMS was cured for 1 h at 70°C. After being removed from the master, the PDMS replica of the channels is sealed to standard microscopy coverslips after plasma oxidation of both PDMS and glass. Liquid connections were incorporated by punching holes with biopsy punchers (WPI). To preventexcessive sticking of silk proteins to the walls of the microfluidic device, a 1% wt/vol solution of F108 block copolymer was introduced into the channels and incubated for 1 h at 60°C (26). Before use, all channels were thoroughly rinsed with 10 mM Tris buffer, pH 8.

Fluid flow during the experiments was controlled by syringe pumps (SP210iw, WPI).

Table 1. Secondary structure content of eADF assemblies

	Structure composition, %		
Protein assembly	Helical (1648–1664 cm^{-1})	β-Sheet (1625–1640 and 1688–1692 cm^{-1})	β-Turn (1665–1685 cm^{-1})
eADF3	55	18	16
eADF3 fiber	31	45	25
eADF4 with phosphate	16	63	21
eADF3 + eADF4 fiber	46	40	13

Infrared spectra were analyzed to determine secondary structure composition of the protein assemblies. eADF3 assemblies generally showed more helical structures than eADF4 assemblies, which revealed a high content of β -sheet structures. Fibers of eADF3 and eADF4 showed β -sheet-rich secondary structure (peak at 1,625 cm^{-1}). However, eADF3 fibers revealed a higher relative content of β -sheet structures than the mixed fibers of eADF3 and eADF4. Details of the structure assignment can be found in Fig. S2. Deviations from 100% result from unassigned spectral regions and from rounding errors.

Microscopy. For optical microscopy, a Zeiss Axiovert 100TV microscope and a Hammamatsu C8484 camera were used. Image analysis and video recording were done with custom-built software [OpenBox (27)]. Scanning electron microscopy (SEM) was performed on a JEOL 840A microscope operated at 15 kV.

Infrared Spectroscopy. Infrared spectra were taken between 7,000 and 1,000 cm^{-1} by using a Bruker IFS66/s spectrometer connected to a Bruker IRscope II infrared microscope with a $\times$36 objective. Dried samples were placed on CaF_2 slides. Spots not covered with protein were used for background measurements. Fibers were localized and then a suiting aperture was chosen, to measure only spectra of fibrous assemblies. Secondary structure elements were assigned by fitting G peaks to the absorbance spectra in the range between 1,580 and 1,700 cm^{-1} (28). A baseline was subtracted from the spectra and a set of Gaussian peaks was fit to the absorption curve. Data analysis was performed by using the PeakFit routine of the Origin software (OriginLab).

Rheology. Rheological characterization of engineered spider silk solutions was performed on a Physica MCR 301 rheometer (Anton Paar). The measurement geometry was a 25 mm cone-and-plate with a sample volume of 160 μl. Temperature of the lower rheometer plate was set to 21°C. A solvent trap was placed over the measurement gap to avoid drying of the sample.

ACKNOWLEDGMENTS. We thank D. Keerl (Technische Universität München) for proteins, M. Hanzlik for electron microscopy, and H. Grabmayr for assistance. S.R. was supported by the CompInt program of the Elitenetzwerk Bayern and by the Bayerische Graduiertenförderung. Support through the International Graduate School of Science and Engineering is also gratefully acknowledged. The work was supported by Deutsche Forschungsgemeinschaft Grants BA 2029/5 (to A.R.B.) and SCHE 603/4-3 (to T.S.), and the support of the Nanosystems Initiative Munich (A.R.B.) and the Munich Center for Integrated Protein Science (T.S.) is gratefully acknowledged.

1. Scheibel T (2005) Protein fibers as performance proteins: New technologies and applications. *Curr Opin Biotechnol* 16:427–433.
2. Vollrath F, Knight DP (2001) Liquid crystalline spinning of spider silk. *Nature* 410:541–548.
3. Jin HJ, Kaplan DL (2003) Mechanism of silk processing in insects and spiders. *Nature* 424:1057–1061.
4. Holland C, Terry AE, Porter D, Vollrath F (2006) Comparing the rheology of native spider and silkworm spinning dope. *Nat Mater* 5:870–874.
5. Vendrely C, Scheibel T (2007) Biotechnological production of spider-silk proteins enables new applications. *Macromol Biosci* 7:401–409.
6. Slotta U, *et al.* (2007) Spider silk and amyloid fibrils: A structural comparison. *Macromol Biosci* 7:183–188.
7. Rammensee S, Huemmerich D, Hermanson KD, Scheibel T, Bausch AR (2006) Rheological characterization of hydrogels formed by recombinantly produced spider silk. *Appl Phys A Mater Sci Process* 82:261–264.
8. Huemmerich D, *et al.* (2004) Primary structure elements of spider dragline silks and their contribution to protein solubility. *Biochemistry* 43:13604–13612.
9. Huemmerich D, Slotta U, Scheibel T (2006) Processing and modification of films made from recombinant spider silk proteins. *Appl Phys A Mater Sci Process* 82:219–222.

10. Slotta U, Tammer M, Kremer F, Koelsch P, Scheibel T (2006) Structural analysis of spider silk films. *Supramol Chem* 18:465–471.
11. Hermanson KD, Huemmerich D, Scheibel T, Bausch AR (2007) Engineered microcapsules fabricated from reconstituted spider silk. *Adv Mater* 19:1810–1815.
12. Exler J, Huemmerich D, Scheibel T (2007) The amphiphilic properties of spider silks are important for spinning. *Angew Chem Int Ed* 46:3559–3562.
13. Vollrath F, Knight DP (1999) Structure and function of the silk production pathway in the spider *Nephila edulis*. *Int J Biol Macromol* 24:243–249.
14. Huemmerich D, *et al*. (2004) Novel assembly properties of recombinant spider dragline silk proteins. *Curr Biol* 14:2070–2074.
15. Lammel A, Schwab M, Slotta U, Winter G, Scheibel T (2008) Processing conditions for spider silk microsphere formation. *ChemSusChem*, in press.
16. Squires TM, Quake SR (2005) Microfluidics: Fluid physics at the nanoliter scale. *Rev Mod Phys* 77:977–1026.
17. Smoluchowski M (1917) Essay of a mathematical theory of the coagulation kinetics of colloidal suspensions (Translated from German). *Z Phys Chem (Frankfurt/Main)* 92:129–168.
18. Guery J, *et al*. (2006) Irreversible shear-activated aggregation in non-Brownian suspensions. *Phys Rev Lett* 96:198301.
19. Tripathi A, Tam KC, McKinley GH (2006) Rheology and dynamics of associative polymers in shear and extension: Theory and experiments. *Macromolecules* 39:1981–1999.
20. Marrucci G, Bhargava S, Cooper SL (1993) Models of shear-thickening behavior in physically cross-linked networks. *Macromolecules* 26:6483–6488.
21. Rousseau ME, Lefevre T, Beaulieu L, Asakura T, Pezolet M (2004) Study of protein conformation and orientation in silkworm and spider silk fibers using Raman microspectroscopy. *Biomacromolecules* 5:2247–2257.
22. Lefevre T, Rousseau ME, Pezolet M (2007) Protein secondary structure and orientation in silk as revealed by Raman spectromicroscopy. *Biophys J* 92:2885–2895.
23. Slotta U, Rammensee S, Gorb S & Scheibel T (2008) Nanofibril and microsphere formation of an engineered spider silk protein. *Angew Chem Int Ed*, in press.
24. Hijirida DH, *et al.* (1996) ^{13}C NMR of *Nephila clavipes* major ampullate silk gland. *Biophys J* 71:3442–3447.
25. McDonald JC, Whitesides GM (2002) Poly(dimethylsiloxane) as a material for fabricating microfluidic devices. *Acc Chem Res* 35:491–499.
26. Hellmich W, *et al*. (2005) Poly(oxyethylene) based surface coatings for poly(dimethylsiloxane) microchannels. *Langmuir* 21:7551–7557.
27. Schilling J, Sackmann E, Bausch A (2004) Digital imaging processing for biophysical applications. *Rev Sci Instrum* 75:2822–2827.
28. Byler D, Susi H (1986) Examination of the secondary structure of proteins by deconvolved FTIR spectra. *Biopolymers* 25:469–487.
29. Rousseau ME, *et al*. (2006) Characterization by Raman microspectroscopy of the strain-induced conformational transition in fibroin fibers from the silkworm *Samia cynthia ricini*. *Biomacromolecules* 7:2512–2521.